IEEE Access
Multidisciplinary | Rapid Review | Open Access Journal

Received July 23, 2020, accepted August 7, 2020, date of publication August 13, 2020, date of current version February 11, 2021.

Digital Object Identifier 10.1109/ACCESS.2020.3016342

Active Flow Control Based on Plasma Synthetic Jet for Flapless Aircraft

XIN WANG[1], JIE YAN[1], JASPREET SINGH DHUPIA[2], AND XIAOSONG ZHU[1]
[1]School of Astronautics, Northwestern Polytechnical University, Xi'an 710072, China
[2]Department of Mechanical Engineering, The University of Auckland, Auckland 1010, New Zealand

Corresponding author: Xin Wang (wangxinfengdz@126.com)

This work was supported by the National Natural Science Foundation of China under Grant 61873210 and Grant 61871302.

ABSTRACT Active flow control (AFC) based on plasma synthetic jet actuator (PSJA) has been attracted a lot of researchers since Anderson and Knight put forward the concept of PSJA for the first time. Since then the characteristic of PSJA has been studied by means of many numerical simulations and experiments. This article showed a series of studies that manipulated a vehicle without moving control surfaces. Firstly, we research the characteristics of the aviation actuator, including the effects of structure and parameters on performance. Secondly, we explore the influence of the actuator on the air field around the aircraft by simulation, including the influence of the actuator on the aerodynamic coefficients and pitching moment coefficient. Finally, since these changes are similar to those caused by the deflection of the rudder surface, we can equivalent the effect of the PSJA to the deflection of the rudder surface, and simulate the three-degree-of-freedom pitch control channel of the aircraft to illustrate the effectiveness of PSJA on the flapless control system.

INDEX TERMS Plasma synthetic jet actuator, active flow control, flapless control system.

I. INTRODUCTION

Due to the great advantages such as small, fast response, more stable and higher efficiency are expected to meet the increasingly challenge of the modern high-performance aircrafts, a synthetic jet produced by PSJA with high velocities (appropriately 300m/s) holds the promise of enabling enhanced flow control. With plasma synthetic jet, it is possible to reduce fluid transition and turbulence, thus making it possible to increase an aircraft's performance whilst at the same time reducing its environmental negative impact.

AFC based on plasma attracted a lot of researchers since Anderson and Knight [1] put forward the concept of plasma synthetic jet (PSJ) for the first time. Chiatto *et al.* [2], [3] improved the structural design of the initial actuator, which not only enhanced the jet formation ability but also increased the working reliability of the actuator. Anderson and Knight [1] and Narayanaswamy *et al.* [4] proposed and improved the one-dimensional theoretical analysis of the PSJ. The results show that the maximum theoretical velocity of the jet has great potential. The numerical calculation models of PSJ were established by Grossman *et al.* [5] and Batey [6] respectively, and the former analyzed the energy utilization efficiency of actuator and the latter expounded the development process of jet. In the field of flight control, Marques and Pascual [7] studied the feasibility of PSJ in flight control. Zhang *et al.* [8] and Torres [9] found that the PSJ has a strong ability to control the high-speed flow field. Seifert *et al.* [22] describes a series of experiments that enabled a flight demonstration of roll-control without moving control surfaces. In addition, Wei *et al.* [23] studied the integration of flight control and flow control at low speed using plasma actuators. In addition, an aircraft has been manoeuvred using supersonic air jet, removing the need for traditional movable flight control surfaces. In [26], designed by UK researchers, a successfully developed UAV using the two 'flap-free' actuators is shown in Fig.1.

The technologies which applying PSJ have potential to improve the performance of flight control systems by replacing moving surfaces with controlled air jet solutions. In summary, active flow control based on PSJA is an important trend in the development of future aircraft. It is worthy to explore the aerodynamic characteristics of the aircraft in the absence of a rudder operation. This article tries to install the PSJA where it is needed to change the air field of the aircraft to achieve wingless flight properly.

The associate editor coordinating the review of this manuscript and approving it for publication was Yingxiang Liu.

FIGURE 1. UK's MAGMA flapless aircraft.

Statement of contributions: in the presented work, a new configuration of plasma synthetic jet model is put forward to form an actuator to aid flight, which is used as a motion auxiliary driver. A two-dimensional numerical simulation aimed at the evolution process of plasma synthetic jet actuator with pulses cycle is carried out. Using an elaborately distributed plasma jet orifice layout on the surface of the vehicle, the aerodynamic coefficients and pitching moment coefficient can be improved, and to illustrate the effectiveness of PSJA on the flapless control system compared with the mechanical flaps only flight vehicle.

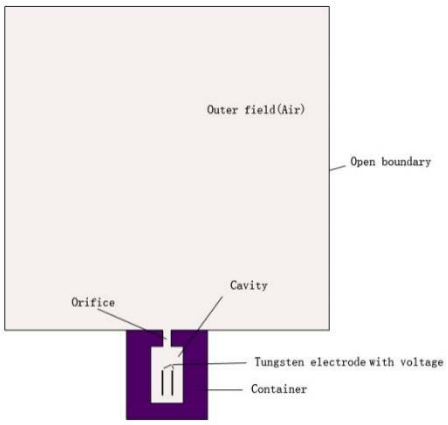

FIGURE 2. Plasma synthetic jet actuator.

II. MATHEMATICAL MODEL

The PSJA as shown in Fig.2 transfers momentum into the external system with zero net mass flow [11]. The working cycle of PSJA mainly consists of three stages: the energy deposition, jet ignition, and the recovery. At the beginning of the PSJA working cycle, a discharge is ignited between the two or three electrodes. This energy deposition rapidly heats the gas in cavity to a high temperature gradually, thus leads to an increase in pressure within the cavity. Air is discharged at a high velocity through orifice in the top of the cavity. The simulation shows that the jet velocity increases greatly in a short period of time and then decreases. At the end of jet ignition phase, the density of air in the PSJA cavity is less than outside. Therefore, ambient air is drawn into the cavity and the spark injector is ready for a next new cycle. Fig.3 shows the above three stages.

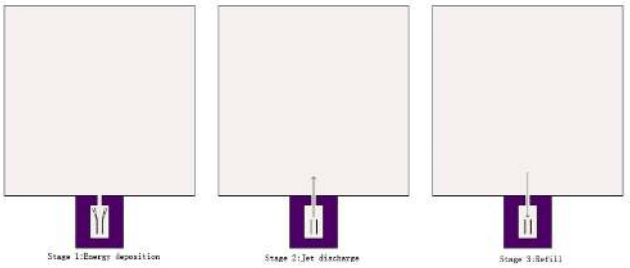

FIGURE 3. Different phases in one working cycle of PSJA.

So far, several reduced-order models with increasing complexity have been proposed. Haack *et al.* [14] proposed the governing equations of the three working phases are derived as one-dimensional partial differential equations. The first Stage is approximated by an instantaneous heating process, This phase is so fast that it is almost instantaneous from the simulation results. while the second Stage is considered to be isentropic. As a result, the model is able to capture blocked or unblocked flow conditions at the nozzle exit, but cannot retrieve the refresh phase, thus limiting its application in the single mode of operation of the actuator. Another attempt by Anderson and Knight [1] analyzed the forces and impulses generated by a single pulse. The model is validated by two-dimensional numerical simulation to derive the explicit relationship between dimensionless energy deposition and pulses. They demonstrated that a series of PSJA generate enough force to replace the aerodynamic surface for flight control.

It is worth mentioning that Zong *et al.* [20] proposed a lumped element model that predicts the entire cycle characteristics and the repeating operating conditions of the actuator. A three-dimensional numerical simulation is performed to define a linear model that describes the heat transfer mechanism between the cavity and the outside field. Consider the case where the two injection phases are assumed to be isentropic or political. The model was validated using experimental data on time-averaged jet total pressure and wall temperature. Later in [17], [21], the model was further improved by combining emissions/heating efficiency with real gas effects.

In addition, Chiatto *et al.* [2], [3] established a three-dimensional model to assess the performance of the designed actuator, and the impact of some parameters like deposited energy and cavity volume was also addressed [12], [13]. Through experiments the peak pressure of the cavity was measured to be about 18 atm, with high-resolution particle image velocimetry (PIV) the propagation of plasma jet was quantified [14].

The above are several important examples to explain the PSJ model. Physical principle of PSJA includes three aspects: one is the ''dynamic effect'', that is, the directional motion of the plasma formed by ionization in the flow field or the plasma added under the action of the electromagnetic field force. The motion of neutral gas molecules is induced by momentum transport between ions and neutral gas molecules,

and the plasma pneumatic excitation is formed. The second is the ''impact effect'', the local temperature and pressure rise (or even shock wave) are produced when some air or applied gas in the flow field is ionized, and the plasma pneumatic excitation is formed. The third is the change of physical properties, the plasma in the flow field changes the density, viscosity and heat conduction of the air flow [15]. The process of PSJA will be discussed in detail below.

A. ENERGY DEPOSITION

In the energy deposition stage, the discharge energy is converted into the internal energy of the gas in a short time, and the gas temperature in the cavity rises sharply. Therefore, the energy deposition process can be modeled as a constant volume heating process. This process is not ideal and exhibits inevitable energy losses due to various electrical and physical effects [16], [17]. In this model, considering the loss associated with the parasitic resistance of the connecting line and the uneven heating effect of the arc discharge, an efficiency factor (η_k) is introduced [19] typically between 20% and 50%. the efficiency factor is essentially the product of the discharge efficiency and the equivalent uniform heating efficiency, $\eta_k = \eta_d \cdot \eta_h$.

When the discharge duration (T_{dis}) is much lower than the time scale (T_h) of the jet discharge, the energy deposition process can be considered transient because a negligible amount of gas will escape from the actuator chamber. Usually this is the case of a capacitor discharge. Considering the typical case where the line inductance and capacitance are on the order of 1μH and 1μF, respectively, the discharge time scale of the capacitor discharge will be O (1μs), which is two orders of magnitude ($O(100\mu s)$) lower than the typical injection time. Therefore, it is reasonable to equate the energy deposition stage model to a constant volume heating process. State variables in the cavity before and after the process (distinguished by superscripts, i and $i+1$) are associated with the following system of equations,

$$\begin{cases} \rho_{ca}^{i+1} = \rho_{ca}^{i} \\ T_{ca}^{i+1} = T_{ca}^{i} + \dfrac{E_h}{C_v V_{ca} \rho_{ca}^{i} T_{ca}^{i}} \\ p_{ca}^{i+1} = p_{ca}^{i} \cdot R(T_{ca}^{i+1}) \cdot T_{ca}^{i+1} \end{cases} \tag{1}$$

where ρ, p and T are the density, pressure and temperature, respectively. Subscripts associated to these symbols indicate the location where these parameters are evaluated, e.g., ca–actuator cavity, e–nozzle exit. $R(T_{ca})$ is the gas constant as a function of cavity temperature to include compressibility effect, i.e., $R(T_{ca}) = R_0 f(T_{ca})$, with R_0 being the air gas constant in standard condition. E_{total} is total energy provided by the power supply system. $E_h = \eta_k \cdot E_{total}$ is the net energy available for gas heating.

B. JET DISCHARGE

In the jet discharge, the initial value of jet velocity is 0 m/s. The gas in the throat is accelerated by the differential pressure between inlet and outlet.

As the airflow in the throat accelerates, the static pressure at the throat inlet begins to decrease. Therefore, the static pressure difference at both ends of the throat decreases, and the airflow acceleration in the throat begins to decrease. When the static pressure at both ends of the throat is equal, the jet velocity reaches the maximum value. As the gas continues to flow out, the total pressure begins to drop down and the density of the air in the cavity decreases. The static pressure at the throat inlet also declines and is less than the ambient pressure. Driven by the differential pressure between the two sides of the throat, the airflow in the throat begins to slow down. When the jet velocity is almost totally reduced, the jet process ends.

During the jet stage, high-pressure fluid exhausts through the orifice, converting its increased internal heat energy into the plasma jet kinetic energy. This phase can be simulated as the discharge process of a reservoir connected to the external ambient by means of a relatively short nozzle or orifice. The application of the mass conservation law to the system composed of the reservoir and the nozzle leads to the following relationship:

$$\frac{d\rho_{ca}}{dt} = -\frac{\rho_e u_e A_e}{V_{ca}} \tag{2}$$

with U_e indicating the exit velocity, A_e the exit orifice area, t the time. The energy equation inside the whole cavity volume is enforced as follows:

$$\left[\rho_{ca}\frac{du_c}{dt} + u_c\frac{d\rho_{ca}}{dt}\right] V_{ca} + \rho_e(h_e + \frac{u_e^2}{2})u_e A_e + \dot{Q} = 0 \tag{3}$$

where u and h are the internal energy and thermodynamic enthalpy, respectively, and $\dot{Q}$ is the total amount of heat power exchanged through the entire surface of the system.

C. REFILL

When the static pressure difference at both ends of the throat is equal to 0 Pa, the jet velocity is not equal to 0 m/s. As the jet continues, the pressure inside the cavity will continue to decrease. After that, the actuator will enter the inspiratory recovery phase. In the refill stage, the ambient atmosphere is sucked into the cavity and mixed with the gas inside the cavity. The final result of mixing is that the density of gas inside the cavity increases, the total pressure increases and the total temperature drops down. In addition, in the mixing process, the heat exchange between inside and outside the cavity also reduces the total temperature of the cavity.

The application of the compressible unsteady Bernoulli's equation, between a point inside the cavity (where the flow velocity is practically null) and the exit section of the nozzle, yields a third equation for these phases:

$$u_c + \frac{p_c}{\rho_c} = u_e + \frac{p_e}{\rho_e} + L_{Th,e}\frac{\partial u_e}{\partial t} + K\frac{|u_e|\,u_e}{2} \tag{4}$$

where K is the head loss coefficient, including entrance/exit losses at exit orifice; $L_{Th,e}$ is the effective length, representing the distance between the two points of application of

Bernoulli's equation. The choice of the values for the head loss coefficient and the effective length has been treated in various previous papers. For piezo-driven synthetic jets, usually these terms have been determined by making a best fitting between numerical and experimental data or by using some empirical expressions [18]. Due to the shortage of literature works on the topic for PSJAs, the previous quantities have been considered as fitting parameters and their values have been determined by matching the results of the lumped model with numerical simulations made with the OpenFOAM code. The effective orifice length has been evaluated as:

$L_{Th,e}/D = L_{Th}/D + \Delta L_{Th,e}$, setting $L_{Th,e} = 1.5$ and K = 1.78, making a best fit with the CFD numerical results. Note that for these simulations, the energy deposition has been assumed instantaneous.

Another convenient equation for the flow along the nozzle is the classic isentropic relationship linking the thermodynamic properties inside the cavity to those at the orifice exit:

$$T_{ca} = T_e \frac{c_p(T_e)}{c_p(T_c)} \left[1 + \frac{\gamma(T_e) - 1}{2} M_e^2\right] \tag{5}$$

where M_e is the exit Mach number, and $\bar{\gamma}$ is the specific heats ratio expressed as a function of the temperature.

The exit flow condition, namely choked or unchoked flow, determines the equation required to close the problem. The establishment of either of these two conditions depends on the critical ratio of the cavity pressure to the exit pressure, i.e.,

$$\frac{p_{ca}}{p_e}|_{cr} = (\frac{\bar{\gamma} + 1}{2})^{\frac{\bar{\gamma}}{\bar{\gamma}-1}} \tag{6}$$

where $\bar{\gamma}$ is the mean value between the two states (i.e., cavity and exit section) involved. If the pressure ratio, after the energy deposition, is greater than or equal to that computed with Equation (6), the flow is choked, otherwise an unchoked regime is assumed. For choked flow, the nozzle exit condition is that the exit Mach number is sonic; otherwise the Kutta condition is retrieved. All the governing equations, written for both the choked and the unchoked case, can be found in [17].

III. NUMERICAL SIMULATION

PSJA is a periodic process when it works normally. With the increase of time, the velocity of the jet increases from small to large, and then decreases gradually after reaching a maximum value, and go to the next loop. However, Affected by other factors, not all cycles are exactly the same. In fact, the efficiency of energy deposition decreases as the number of cycles increases.

The evolution process of PSJ in static air environment is demonstrated in Fig.4, when the air temperature is 173.15K and the air pressure is 0.01 atm. At the beginning of 70μs, the velocity of the nozzle increases gradually, when t = 70μs, and the injection speed is the highest, which can reach 303 m/s. the air flow begins to flow back into the cavity and enter the next cycle.

When the first cycle is over, there is a tendency for the airflow to flow back. The size of the cycle is closely related

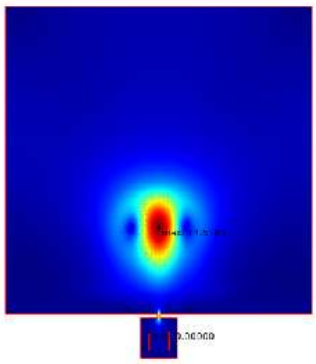

FIGURE 4. Jet velocity contour.

to the frequency. The simulation shows that the second jet velocity does not have a large attenuation when the period T is 400μs. This means that the airflow has sufficient reflow time during this time and does not affect the subsequent velocity (As shown in Fig.5, jet speed reaches 303m/s). The jet velocity map of the second cycle is as follows (when t = 470μs).

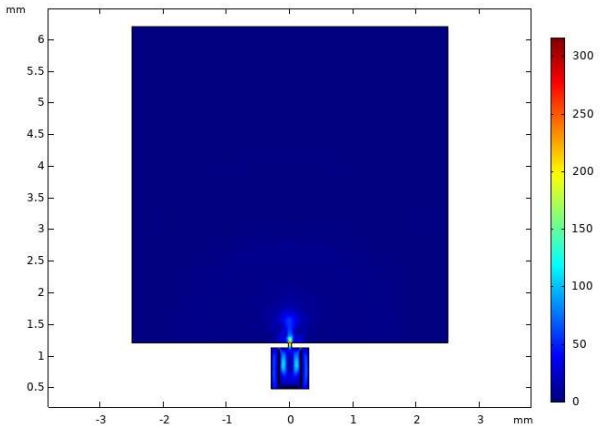

FIGURE 5. Second jet velocity when t = 470μs.

In addition, changing the structural parameters of the actuator, such as working voltage, temperature and other parameters can change the velocity of the jet, and then control the state of the air flow around vehicles. In many other literatures, the jet velocity is roughly on the magnitude of hundred meters per second. Different parameters have different effects on the jet velocity. For example, as the frequency increases, the third-stage airflow cannot be reflowed in time, resulting in insufficient air at the subsequent eruption and the jet velocity becomes smaller. The performance that affects PSJA is not only the speed of the jet, but also the size of the vortex in the cloud, the latter is also an important indicator to determine the performance of the actuator.

IV. PLASMA FLOW CONTROL METHOD

The 3D model of the flight vehicle of interest is shown in Fig.6. For UAV vehicles, the traditional rudder wing actuation mechanism has a long response time (100∼500ms).

FIGURE 6. Flight vehicle schematic.

Meanwhile, as the height increases, the efficiency of the rudder surface drops sharply. The combined control technology using aerodynamic/direct force is almost an inevitable choice for aircraft with high maneuverability [10]. The PSJA is usually mounted at the leading edge or anywhere to improve the aerodynamics around the aircraft. Many researchers have confirmed the effectiveness of PSJA by enhanced lift coefficient and decreasing drag coefficient.

This article intends to load the actuator on a UAV aircraft. According to the influence of the jet on the flow field and the research results of the plasma synthesis jet in the early stage of the research group, the saturation period of the jet is about 0.4ms. In the ejection phase, the jet has a significant impact on the flow field, and the time interval is very short, about 0.1ms. During this time period, it can be assumed that the mass flow of the jet is a certain value, and the actuator outlet is defined as the mass flow boundary. In the backfilling phase, the actuator has little effect on the external flow field, and the exit of the actuator in the backfill phase can be defined as the object boundary condition without considering the action of the actuator. Based on the above analysis, the plasma synthesis jet is simplified into a pulse jet for simplifying the numerical simulation of the flow field control model [25].

A. CONTROL MODELS

The rate of pitch from PSJA is found by the conservation of angular momentum about the center of gravity of the flight vehicle

$$\frac{d^2\theta_{PSJA}}{dt^2} I = M_{pitch} \tag{7}$$

where I is the moment of inertia about the center of gravity of the vehicle, θ is the angle of rotation, and M_{pitch} is torque at the center of gravity. Integrating from t = 0 to t, we can obtain

$$\frac{d\theta_{PSJA}}{dt} = \frac{R}{I} P_{PSJA} \tag{8}$$

where P_{PSJA} is the dimensional impulse. For an array of N plasma jets located approximately at a distance R from the center of gravity [27].

From the definition of dimensionless impulse and dimensionless energy deposition, the impulse P_{PSJA} can be given by

$$\sqrt{\gamma \varepsilon} \vartheta K = P_{PSJA} \tag{9}$$

where ε is the measure of the magnitude of the energy deposited, γ is the ratio of specific heats, ϑ is the dimensionless energy-deposition rate, and K is the internal energy deposit in the cavity.

The total aerodynamic pitch moment is given by the following equation:

$$M_{pitch} = \begin{bmatrix} m_z + C_y (X_T - X_t)/b_A + \\ Ke(X_t - L_P)/b_A \end{bmatrix} qSb_A \tag{10}$$

where m_z is the pitching moment coefficient, b_A is the lateral-directional reference length, X_t is the distance between dynamic pressure point and centroid, X_T is the reference centroid, and L_p is the distance between rudder axis and centroid. Ke denotes the PSJA equivalent deflection angle, q is the dynamic pressure, S is the reference area, and b_A is the lateral-directional reference length.

To predict both the single cycle and the repetitive working process of the PSJA device, an analytic model was described by Zong *et al.* [20]. Chiatto and de Luca [21] presented a lumped-element model (LEM) to demonstrate the temporal evolution of a plasma synthetic jet. In view of the experimental verification of the effectiveness of the actuator in control of the rolling channel of low-speed aircraft [24], we intend to use the model to verify the effect of the actuator on the aircraft's pitch channel by an elaborately distributed plasma jet orifice layout on the nose surface of the vehicle.

The specific steps are as follow, actuators are arranged in a row on the head of the airfoil. A few of actuators are sprayed upwards at a speed of 500 m/s at the beginning of the jet. Fig.7 shows the velocity cloud after the actuator is added. It can be seen that the jet has a certain degree of disturbance to the flow field around the aircraft.

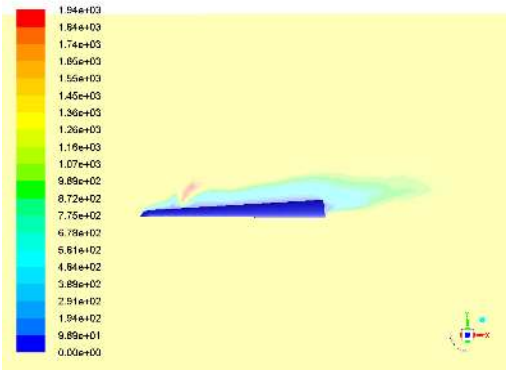

FIGURE 7. Flight vehicle flow field variation profile.

We get the pitch coefficient curve at different angles of attack and Cl/Cd curve. Fig.8 shows the curve of the lift coefficient as a function of the angle of attack. It can be seen from the Fig.8 that the action of the actuator causes the lift coefficient to be reduced to some extent. Fig.9 is a diagram of drag coefficient with angle of attack changes. It can be seen from the figure that before the angle of attack is 20 degrees, the actuator can reduce the drag coefficient to some extent, and the reduction of the drag coefficient is more significant at small angle of attack. However, when the angle of attack is larger than 20 degrees, the actuator cannot be used.

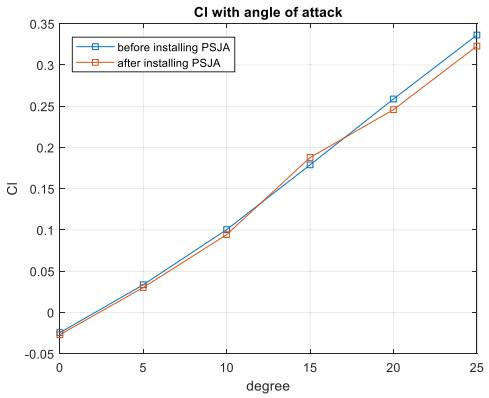

FIGURE 8. Cl curve with angle of attack.

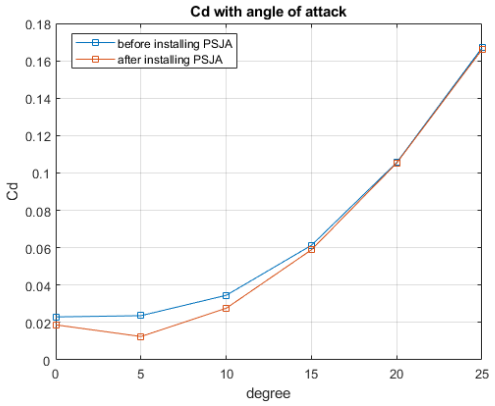

FIGURE 9. Cd curve with angle of attack.

B. CONTROL METHOD

The control mechanism of plasma synthesis jet can be summarized into the following three aspects:

(1) The jet stream increases the thickness of the turbulent boundary layer near the wall, the turbulence intensity and the energy deposition, which improves the ability of the boundary layer to suppress the flow separation, reduces the size of the separation zone, and reduces the shock layer intensity.

(2) The increase of jet temperature increases the local sound velocity in the near-wall jet region, reduces the local air speed, and raises the sound velocity. The heat blocking effect of gas heating increases the mass flow of gas outside the jet region, causing compression of the bow shock, causing the bow shock to be convexly deformed.

(3) The introduction of the jet interference shock wave will cause the pressure difference before and after the arc shock in the flow field around the cylinder to decrease, thereby reducing the shock layer intensity.

The control method can be summarized as:

1) The surface pressure on the control surface is symmetric except at the PSJA orifice.

2) The axis of the plasma jet is perpendicular to the moment arm.

3) The flow is inviscid, and heat transfer is not negligible.

4) The distance from the center of gravity of the flight vehicle to the PSJA is much larger than the diameter of the plasma jet.

The analysis determines the feasibility of using the PSJA to control the pitching moment of a flight vehicle. The PSJA and aerodynamic control surface are compared on the time scale on the order of the plasma jet discharge.

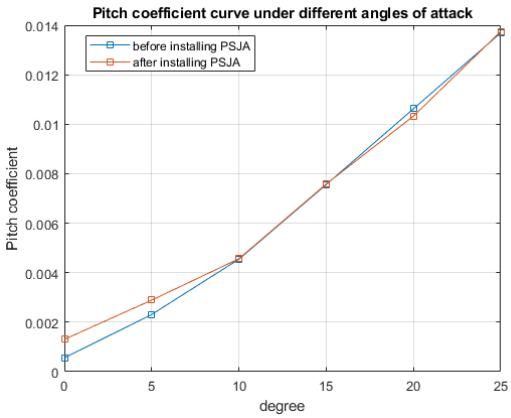

FIGURE 10. Cm curve with angle of attack.

C. EFFECTIVENESS OF PARAMETERS

It also can be seen from the Fig.10 that after installing PSJA, when the angle of attack is less than 10 degrees, the pitching moment coefficient is increased to some extent, and the closer to 10 degrees, the smaller the amplitude is. However, when the angle of attack is between 15 and 20 degrees, the pitching moment coefficient becomes smaller. Regardless of increasing or decreasing, it can be equivalent to a certain angle of deflection of the rudder surface. This means that the maximum deflection angle and the maximum output torque of the rudder surface are increased to some extent, and if the performance of the actuator is increased, the dynamic response process of the aircraft is also improved.

We will verify the effect of this upgrade on the flight control system subsequently. The motion model of the vehicle can be divided into two groups of longitudinal and lateral equations in the flight control system, ignoring the interaction between longitudinal and lateral systems. The longitudinal motion only involves longitudinal motion parameters and aerodynamic forces, and aerodynamics are generally accustomed to using velocity coordinates. Therefore, it is convenient to describe the longitudinal motion of the vehicle using velocity coordinates.

The above simulation is only to make the jet equivalent to a pulse jet, and the actual situation is more complicated. The size of the jet and the size of the vortex are constantly changing in one cycle. Generally, in one cycle about 0.4ms, the flow field passes through the initial state, the flow field changes after the jet is started, and the jet is closed. The field can be restored and recovered to its original initial state, indicating that the jet has certain timeliness for the control of the flow field. Only when the frequency of the jet reaches

a certain value can the complete control of the flow field be realized.

The longitudinal motion of the aircraft consists of the translational motion of the aircraft's centroid in the plane of flight or the plane of symmetry $x_1O_1y_1$ and the rotation of the aircraft about the Oz_1 axis. In longitudinal motion, $V, \theta, \varphi, \alpha, \omega_{z1}, x, y$ is a function of time and also commonly referred to as longitudinal motion parameters. The parameter $\beta, \gamma, v, \psi, \sigma, \omega_{x1}, \omega_{y1}, z$ equal to zero in the longitudinal motion is the lateral motion $\beta, \delta_x, \delta_y$ parameter, and the lateral motion is composed of the translation of the aircraft along the Ox_1 axis and the rotation of the Oy_1 axis around the Ox axis.

In the absence of lateral motion (no yaw, roll operation, and no lateral interference), longitudinal motion can exist independently; However, lateral motion cannot exist separately from longitudinal motion. Therefore, in order to separate the longitudinal motion from the lateral motion, the following assumptions must be met:

1) Lateral motion parameter $\beta, \gamma, v, \psi, \sigma, \omega_{x1}, \omega_{y1}, z$ and rudder angle, δ_x, δ_y is a small amount, so there is $\cos\beta \approx \cos\gamma \approx \cos v \approx 1$, and the products of small quantities such as $\sin\beta \sin\gamma$, $\omega_y \sin\gamma$, $\omega_x\omega_y$ and $Z \sin v$ etc. The C pairs can be omitted.

2) The aircraft flies in a certain vertical plane basically, and its flight trajectory is not much different from the trajectory in the vertical plane.

3) The deflection of the pitch control mechanism only relies on the longitudinal motion parameters, and the yaw and roll are only dependent on the lateral motion parameters.

Using the above assumptions, the equations of motion of the aircraft can be composed of equations describing longitudinal motion and equations describing lateral motion. The equations describing the longitudinal motion of the aircraft are:

$$\begin{cases} \dot{x} = V\cos\theta \\ \dot{y} = V\sin\theta \\ \dot{V} = \dfrac{1}{m}(-X - mg\sin\theta) + \dfrac{1}{m}\left(T_{x1}\cos\alpha - T_{y1}\sin\alpha\right) \\ \dot{\theta} = \dfrac{1}{mV}(Y - mg\cos\theta) + \dfrac{1}{mV}\left(T_{x1}\sin\alpha + T_{y1}\cos\alpha\right) \\ \dot{\omega}_{z1} = \dfrac{M_{Tz} + M_R}{I_z} \\ \dot{\varphi} = \omega_{z1} \\ \alpha = \varphi - \theta \\ \dot{m} = -\dot{m}(t) \\ \delta_z = f(u) \end{cases} \tag{11}$$

The longitudinal motion has nine equations, including nine unknown parameters, which can be solved in a closed manner.

V. NUMERICAL SIMULATION RESULTS AND DISCUSSION

A. NUMERICAL SIMULATION

Numerical flight simulation is based on the motion of the aircraft. It is a combination of system simulation technology, computer technology and aviation technology. It has advantage such as quick effect, low cost, safety, reliability and reusability. The motion of the aircraft in space is a six-degree-of-freedom motion, including constant level flight, climb and fall, pitch motion, yaw angle change, and roll motion. The simulation is carried out by inputting the basic flight data, aerodynamic parameters and attitude control parameters of the aircraft into the simulation software, and observe the control effect of the actuator on the pitch attitude of the non-rudder aircraft.

The speed of the aircraft we use is above 100m/s, and the control effect must be improved to practical application value. Therefore, it is necessary to optimize the arrangement position of the actuator or to use a plasma actuator in the form of a more efficient nanosecond pulse discharge. By adopting the nanosecond pulse discharge mode, the energy can be released in a short time, thereby generating strong pulse disturbance or even shock wave disturbance in the flow field, also improving the ability to induce the vortex and promote the blending of the boundary layer with the mainstream. For example, the literature [15] uses a nano-second pulse driven dielectric barrier discharge plasma oscillator. For the reason that based on the improvement of plasma flow control efficiency, plasma flow control technology can be a new type of flight control.

As mentioned above, the installation of an actuator at a specific location on the surface of the aircraft changes the flow field around the aircraft. Here we verify through simulation that the changed parameters have at least lift coefficient, drag coefficient and pitching moment coefficient.

In Fig. 8, Fig. 9 and Fig. 10, the angle of attack varies from 0 to 25°. When the angle of attack is 5° and the Mach number is 0.5, the lift coefficient decreases by 0.001, the drag coefficient decreases by 0.006, and the pitching moment coefficient increases by 0.0006. The change of these parameters is similar to the change of the aerodynamic parameters of a certain type of aircraft when the rudder surface is deflected by 2° under the same conditions. In other literatures, the same equivalent method is used to illustrate the actuator-based main flow control without rudder bias.

The change in these parameters is equivalent to a horizontal rudder deflection at a certain angle. Therefore, in order to explain the function of the actuator, it can be achieved by changing the rudder bias in the control system. A flight simulation of the horizontal rudder deflection of 2° (downward positive) was performed. The simulation duration was 10 seconds, the initial height was 18000m It can be seen from Fig.11 that the 2° aileron rudder bias is applied within 2 to 4 seconds, and the pitch angle signal curve of Fig.12 is observed. It can be seen that the pitch angle of the aircraft has a process of first reduced and then increased to the original level. This indicates that the non-rudder aircraft has good

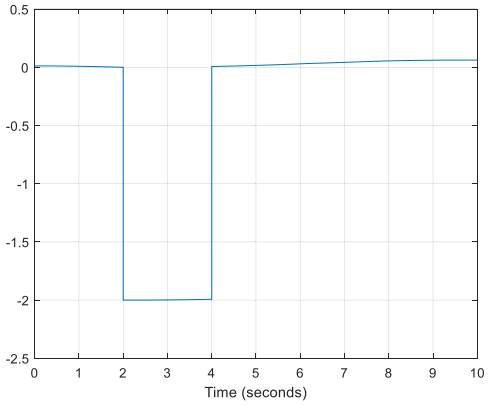

FIGURE 11. Equivalent deflection angle with time.

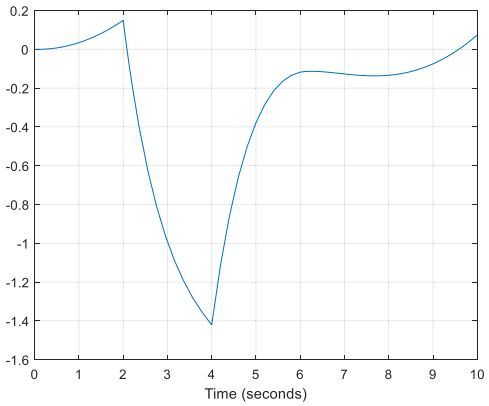

FIGURE 12. Pitch angle curve with time.

lateral stability and has a tendency to return to the initial pitch attitude after being disturbed. The flying height is first increased slightly and then decreased as shown in Fig.13. The above parameters are changed based on the deflection of the rudder surface, and the action of the stimulator can be equivalent to the deflection of the rudder surface. So it can be seen that the impact of the actuators on the aircraft.

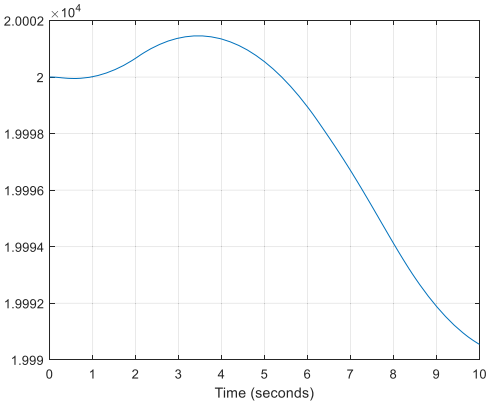

FIGURE 13. Flight altitude versus time curve.

When the PSJA equivalent rudder angle is deflected by 2°, we can know from the above formula that φ will increase to some extent; as the lift coefficient increases, the drag coefficient drops down, the lift Y increases, and the resistance X decreases. As a result, the θ decreases to a certain extent, and the α increases, and the centroid coordinates (x, y) of the aircraft are both increased. When the deflection disappears, the above parameters are restored to the size at the beginning. The speed V and the flight altitude h are all decreased, and (x, y) is gradually getting smaller.

B. COMPARISON WITH OTHER METHODS

First, the related work by Anderson and Knight [27] stated that plasma jet is sensitive to geometry, and is not well predicted by the one-dimensional analytical result. In our work, we put forward a two-dimensional numerical simulation (Fig. 5) aimed at the evolution process of plasma synthetic jet actuator with pulses cycle due to its highly transient nature. In [27], it is shown through an analysis that the effectiveness index parameter versus vehicle Mach number can be improved and can reach deflection operational efficiency rate of 0.1. In our study, the maximum operational efficiency λ can be achieved by maximum pitch angle divided by PSJA equivalent deflection angle, and shown in Fig. 11 and Fig. 12 at time

$$t = 4s, \quad \lambda_{\max} = \frac{|-1.4\,\text{deg}|}{2\,\text{deg}} = 0.7.$$

Second, we compare with the study by Li *et al.* [28]. There are problems in the application of plasma synthetic jet actuators in flight active flow control, and one of them is low electric energy conversion efficiency. In [28], it is reported a maximum plasma jet velocity at 103.08m/s. In this work, from Fig. 5 we can see that the plasma jet speed reaches 303m/s with higher energy conversion efficiency. Our work shows some advantage that it is recommended to use in a case of the maneuver orientation for the reference. This means PSJA has potential to produce sufficient force to replace an aerodynamic surface for flapless flight control.

VI. CONCLUSION

The main content of this article is based on the active flow control of PSJA to reach the goal of the control of the pitch channel of the aircraft. First, we discuss some characteristics of the PSJA, including the effects of various parameters of the actuator on the jet velocity. Secondly, we add the actuator to the surface of the aircraft and discuss how to influence the parameters of the aircraft control system. Finally, we combined the control system to simulate the effect of the actuator. Through data analysis, we can conclude that the control effect of the actuator on the aircraft is considerable to some extent. Especially in some special occasions, when we are troubled by the so-called passive flow control method, we can find some improvements here.

Due to the wide range of applications of plasma, and the continuous development, the shape of the actuator, the installation location and the incentive method affect our final results. There are still many aspects for improvement. Subsequent effects on yaw and rollover channels are also not negligible. In this article, we need to put in a certain amount

of energy to get more data to prove the role of the actuator. There are a lot of advantages in the absence of rudder flight, and it is also one of the development directions of active flow control in the future.

REFERENCES

[1] K. V. Anderson and D. D. Knight, "Plasma jet for flight control," *AIAA J.*, vol. 50, no. 9, pp. 1855–1872, Sep. 2012.

[2] M. Chiatto, A. Palumbo, and L. de Luca, "A calibrated lumped element model for the prediction of PSJ actuator efficiency performance," *Actuators*, vol. 7, no. 1, p. 10, Mar. 2018.

[3] M. Samimy, I. Adamovich, B. Webb, J. Kastner, J. Hileman, S. Keshav, and P. Palm, "Development and characterization of plasma actuators for high-speed jet control," *Exp. Fluids*, vol. 37, no. 4, pp. 577–588, 2004.

[4] V. Narayanaswamy, L. L. Raja, and N. T. Clemens, "Characterization of a high-frequency pulsed-plasma jet actuator for supersonic flow control," *AIAA J.*, vol. 48, no. 2, pp. 297–305, Feb. 2010.

[5] K. Grossman, C. Bohdan, and D. VanWie, "Sparkjet actuators for flow control," in *Proc. AIAA Paper*, 2003, p. 57.

[6] A. Batey, "UK's magma UAV to demonstrate flapless fluidic flight control," *Aviation Week Space Technol.*, vol. 180, no. 5, pp. 44–45, 2018.

[7] P. Marques, "Aerodynamics of UAV configurations," in *Advanced UAV Aerodynamics, Flight Stability and Control*. Hoboken, NJ, USA: Wiley, 2017.

[8] X. Zhang, Y. Huang, P. Yang, P. Zhang, Z. Huang, D. Wang, and H. Li, "Flight test of flow separation control using plasma UAV," *Acta Aeronauticaet Astronautica Sinica*, no. 2, pp. 121587-1–121587-8, 2018.

[9] A. J. C. Torres, "Flow structure modification using plasma actuation for enhanced UAV flight control," in *Advanced UAV Aerodynamics, Flight Stability and Control*. Hoboken, NJ, USA: Wiley, 2017.

[10] Z. Su, J. Li, H. Liang, B. R. Zheng, B. Wei, J. Chen, and L. K. Xie, "UAV flight test of plasma slats and ailerons with microsecond dielectric barrier discharge," *Chin. Phys. B*, vol. 27, no. 10, pp. 459–468, 2018.

[11] G. Yang, Y. Yao, J. Fang, T. Gan, Q. Li, and L. Lu, "Large-eddy simulation of shock-wave/turbulent boundary layer interaction with and without SparkJet control," *Chin. J. Aeronaut.*, vol. 29, no. 3, pp. 617–629, Jun. 2016.

[12] M. Seyhan and Y. E. Akansu, "The effect of a novel spark-plug plasma synthetic jet actuator on the performance of a PEM fuel cell," *Int. J. Heat Mass Transf.*, vol. 140, pp. 147–151, Sep. 2019.

[13] B. Cybyk, K. Grossman, and J. Wilkerson, "Performance characteristics of the SparkJet flow control actuator," in *Proc. 2nd AIAA Flow Control Conf.* Portland, OR, USA: AIAA, Jun. 2004, p. 2131.

[14] S. Haack, T. Taylor, J. Emhoff, and B. Cybyk, "Development of an analytical SparkJet model," in *Proc. 5th Flow Control Conf.* Chicago, IL, USA: AIAA, Jun. 2010, p. 4979.

[15] Y. Wu and Y. Li, "Progress and outlook of plasma flow control," *Acta Aeronautica et Astronautica Sinica*, vol. 36, no. 2, pp. 381–405, 2015.

[16] S. H. Popkin, B. Z. Cybyk, C. H. Foster, and F. S. Alvi, "Experimental estimation of SparkJet efficiency," *AIAA J.*, vol. 54, no. 6, pp. 1831–1845, Jun. 2016.

[17] H. Zong, Y. Wu, H. Song, and M. Jia, "Efficiency characteristic of plasma synthetic jet actuator driven by pulsed direct-current discharge," *AIAA J.*, vol. 54, no. 11, pp. 3409–3420, Nov. 2016.

[18] L. de Luca, M. Girfoglio, M. Chiatto, and G. Coppola, "Scaling properties of resonant cavities driven by piezo-electric actuators," *Sens. Actuators A, Phys.*, vol. 247, pp. 465–474, Aug. 2016.

[19] H. Zong, M. Chiatto, M. Kotsonis, and L. de Luca, "Plasma synthetic jet actuators for active flow control," *Actuators*, vol. 7, no. 4, p. 77, Nov. 2018.

[20] H.-H. Zong, Y. Wu, Y.-H. Li, H.-M. Song, Z.-B. Zhang, and M. Jia, "Analytic model and frequency characteristics of plasma synthetic jet actuator," *Phys. Fluids*, vol. 27, no. 2, Feb. 2015, Art. no. 027105.

[21] M. Chiatto and L. de Luca, "Numerical and experimental frequency response of plasma synthetic jet actuators," in *Proc. 55th AIAA Aerosp. Sci. Meeting*, Grapevine, TX, USA, Jan. 2017, pp. 9–13.

[22] A. Seifert, S. David, I. Fono, O. Stalnov, and I. Dayan, "Roll contrial via active flow control: From concept to flight," *J. Aircr.*, vol. 47, no. 3, pp. 864–874, May 2010.

[23] Q. Wei, Z. Niu, B. Chen, and X. Huang, "Bang-bang control applied in airfoil roll control with plasma actuators," *J. Aircr.*, vol. 50, no. 2, pp. 670–677, Mar. 2013.

[24] H. Du, Z. Shi, X. Geng, and D. Wei, "Experimental study of directional-lateral aerodynamic moment control of micro air vehicle by plasma actuator," *Acta Aeronautica et Astronautica Sinica*, vol. 33, no. 10, pp. 1781–1790, 2012.

[25] L. Wang, Z. Xia, Z. Luo, and Y. Zhang, "Effect of pressure on the performance of plasma synthetic jet actuator," *Sci. China Phys., Mech. Astron.*, vol. 57, no. 12, pp. 2309–2315, Dec. 2014.

[26] *UK's Magma UAV To Demonstrate Flapless Fluidic Flight Control*. Accessed: Feb. 22, 2018. [Online]. Available: https://aviationweek.com/defense-space/uks-magma-uav-demonstrate-flapless-fluidic-flight-control

[27] K. V. Anderson and D. D. Knight, "Plasma jet for flight control," *AIAA J.*, vol. 50, no. 9, pp. 1855–1872, Sep. 2012.

[28] J. Li and X. Zhang, "Active flow control for supersonic aircraft: A novel hybrid synthetic jet actuator," *Sens. Actuators A, Phys.*, vol. 302, Feb. 2020, Art. no. 111770.

XIN WANG is currently an Associate Professor with Northwestern Polytechnical University, China. His current research interests include design and simulation of hardware-in-the-loop test equipment, photoelectric detection, and control engineering theory.

JIE YAN, photograph and biography not available at the time of publication.

JASPREET SINGH DHUPIA, received the B.Tech. degree from the Indian Institute of Technology Delhi, India, and the M.S. and Ph.D. degrees from the University of Michigan, Ann Arbor, MI, USA, in 2004 and 2007, respectively. He has been with The University of Auckland, New Zealand, since 2015.

XIAOSONG ZHU, photograph and biography not available at the time of publication.